Temporal Fluctuation of Backscattered Field Due to Bioturbation in Marine Sediments

Christopher D. Jones and Darrell R. Jackson

Applied Physics Laboratory
University of Washington, HN-10
Seattle, WA, 98105, USA
E-mail: cjones@apl.washington.edu, drj@apl.washington.edu

Abstract

Biological activity in marine sediments creates a time-varying, randomly fluctuating medium. A bio-diffusive model is proposed for predicting the temporal and spatial spectrum of sediment density fluctuations. Perturbation theory is used to model sediment volume scattering and the temporal correlation of the scattered field. These models are compared with field data recorded in a biologically active shallow water environment, and sediment bio-diffusion parameters are estimated.

1. Introduction

Biologically active sediments are continually modified by epifauna (organisms that live on the sediment surface) and infauna (organisms living in the sediment). The collective mixing effect of these organisms is termed bioturbation. On micro- and macroscopic scales, bioturbation affects the physical and chemical properties of the sediment. The intensity of bioturbation affects the distribution of marine chemicals which in turn influences the microbial activity in the sediment and the ultimate fate of marine pollutants [1, 2]. Epifaunal activity creates microtopography that may decrease the critical velocity necessary to erode surface layers [3]. Infaunal activity, such as tube building, is responsible for vertical and horizontal redistribution of solid material within the sediment, creating spatial and temporal inhomogeneities in sediment bulk properties (e.g. density and porosity). Often, the traces of these mixing activities provide the only evidence of the existence of fauna in an area [3].

Models of acoustic scattering from the sea floor can be used to invert for sediment properties such as roughness spectra and volume inhomogeneity spectra [5, 6, 7]. In such inversions it is assumed that the sea floor does not change with time, however, on time and distance scales comparable with with scales of bioturbation, acoustic properties of the sea floor will change. Time scales of bioturbation range from diurnal to seasonal, and distances scales range from mesoscale to meter scale patchiness [1].

In this paper, the effects of bioturbation on acoustic backscatter will be discussed. A stochastic model of bioturbation will be introduced, and a review of perturbation theory to model volume backscatter presented. By coupling these models, a model for the decorrelation of an acoustic backscattered field due to bioturbation is obtained. Model predictions will be compared with field data recorded in a biologically active shallow water environment over a two month period.

2. Bio-diffusive Sediment Model

Quantitative analysis of bioturbation requires the use of mathematical models that describe the mixing process. The simplest model of this mixing process is the vertical diffusion equation [1, 2, 4].

$$\frac{\partial}{\partial t}c(z,t) - D_b\nabla^2 c(z,t) = 0 \tag{1}$$

This equation describes the temporal and spatial evolution of a tracer concentration, $c(z,t)$, deposited on the surface of the sediment and being mixed into the sediment by localized diffusion. In this model all the biological

activity is described by a single parameter, the bio-diffusion coefficient D_b. The diffusive nature of the mixing process is not the result of the mixing effects of a single type of organism, but is rather the net effect of a collection of infauna having a wide range of mixing lengths and acting over a long period of time.

While the behavior of a sediment tracer (such as a radio-isotope) may be modeled by the homogeneous and steady-state solution of the one dimensional diffusion equation, in the context of acoustic scattering, the inhomogeneous and transient nature of the process is of primary concern. On the time scales of interest, the movement of sediment is not necessarily restricted to localized mixing between adjacent horizontal layers, rather, larger organism may transfer sediment between non-adjacent layers creating nonlocal (non-diffusive) mixing that give rise to spatial inhomogeneity. Furthermore, over short time periods it cannot be assumed that a large collections of organisms with a broad spectrum of sizes have reworked the sediment. Instead, mixing may be dominated by organisms with discrete length scales.

Given that we are interested in this nonlocal and transient behavior of bioturbation, the simple diffusion model is inadequate. A proposed extension to (1) is the forced diffusion process, generalized in terms of the sediment bulk density ρ_s.

$$\frac{\partial}{\partial t}\rho_s(\mathbf{r},t) - \nabla \cdot [D(\mathbf{r},t)\nabla\rho_s(\mathbf{r},t)] = g(\mathbf{r},t) \tag{2}$$

Here, D is a local diffusion coefficient representing the continuous diffusive activity of smaller organisms (meiofauna) or the collapsing and filling of borrows created by larger organisms. By taking D to be a scalar, we have assumed isotropic diffusion. In general, the horizontal and vertical diffusion rates may differ [1] and a tensor diffusion coefficient must be used. The right-hand side of (2) is an excitation function that represents the nonlocal mixing activities of larger organisms (macrofauna).

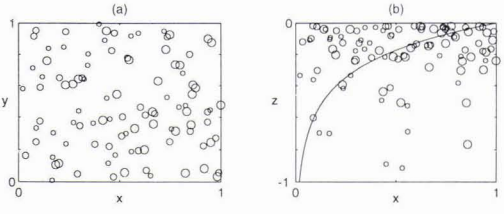

Figure 1: Sediment source and sink functions randomly distributed in the (a) horizontal and (b) vertical directions. The depth-dependent point density, $\lambda(z)$, is plotted as the solid line in (b). The $z = 0$ plane is the sediment-water interface.

If there is a single transport event at time t_n that removes or deposits sediment at a small volume centered at $\mathbf{r}_n$, then the excitation function can be modeled as a series of impulsive source and sink events occurring randomly in space and time.

$$g(\mathbf{r},t) = \sum_n q_n h_n(\mathbf{r}-\mathbf{r}_n)\delta(t-t_n) \tag{3}$$

The function h_n describes the random size and shape of the volume of sediment moved by each event. The coefficient q_n is a zero-mean random variable that represents the amplitude of each event, therefore, mass is conserved within the volume of interest.

In general, the excitation may be anisotropic and inhomogeneous in space. For example, biological activity may decrease with depth into the sediment, as illustrated by Figure 1. This figure shows a hypothetical depth-dependent distribution of spherical shape functions. Activity is concentrated near the sediment-water interface and decreases with depth into the sediment, but is uniform in the horizontal plane. In this paper we will assume spatial homogeneity in the horizontal plane but include the effects of depth dependent mixing activities.

Equation (2) is a deterministic differential equation with a random excitation, g, due to the nonlocal exchange of sediment. The solution, ρ_s, can then be interpreted as the output of a linear system with a stochastic input. Thus the mixing process can be characterized as a linear filtering process where the spectrum, $S_{\rho\rho}$, of the output process is defined completely in terms of the spectrum, S_{gg}, of the input and the frequency response, $H_D(\mathbf{k},\omega)$, of the linear system representing the left hand side of (2).

$$S_{\rho\rho}(\mathbf{k},\omega) = |H_D(\mathbf{k},\omega)|^2 S_{gg}(\mathbf{k},\omega) \tag{4}$$

If t_n and $\mathbf{r}_n$ are Poisson random variables, the spectrum of the input process is found by interpreting the excitation as the output of a filtered Poisson, or shot-noise process [8]. The depth dependence of g will be characterized by the number of events per unit volume and time at each depth, that is, the depth-dependent Poisson point density $\lambda(z)$ (Figure 1). If the point density is a slowly varying function of depth relative to the shape function, it follows that the autocorrelation of g can be expressed in terms of the autocorrelation, R_{hh}, of the shape function,

$$R_{gg}(\mathbf{r}_d, z, \tau) \simeq \sigma_q^2 \lambda(z) \langle R_{hh}(\mathbf{r}_d)\rangle \delta(\tau) \ , \tag{5}$$

where σ_q^2 is the variance of q_n. The correlation is expressed in terms of the difference coordinates $\mathbf{r}_d = \mathbf{r}_1 - \mathbf{r}_2$ and $\tau = t_1 - t_2$, therefore, the excitation can be considered a depth-dependent, locally stationary random process.

The shape function is random in general and the expected value of its autocorrelation is used. The spectrum is found by taking the Fourier transform of (5) with respect to $\mathbf{r}_d$ and τ,

$$S_{gg}(\mathbf{k}, z, \omega) \simeq \frac{\sigma_q^2}{2\pi} \lambda(z) S_{hh}(\mathbf{k}) \ , \tag{6}$$

where $S_{hh}(\mathbf{k}) = (2\pi)^3 \langle |H_n(\mathbf{k})|^2 \rangle$ is the expected value of the shape function spectrum, and H_n is the Fourier transform of the shape function h_n. Note that the spectrum is independent of temporal frequency, ω, because of the assumed impulsive nature of the source and sink events.

For the case of a depth-dependent and isotropic diffusion coefficient, the system frequency response can be approximated as

$$H_D(k, \omega) \simeq \frac{1}{D(z)k^2 - i\omega} \ , \tag{7}$$

where $k^2 = k_x^2 + k_y^2 + k_z^2$ and the gradient of $D(z)$ is neglected. Combining (4-7) and performing an inverse Fourier transform in time, the temporal correlation / spatial spectrum of density inhomogeneities in the sediment can be modeled as

$$S_{\rho\rho}(\mathbf{k}, z, \tau) = \sigma_q^2 \frac{\lambda(z)}{D(z)} \frac{S_{hh}(\mathbf{k})}{2k^2} e^{-D(z)k^2|\tau|} \ . \tag{8}$$

The above expression is general in the sense that it attempts to model bioturbation in nonspecific terms (e.g. diffusion and point density) while still accounting for the two-scale nature of the mixing process (meiofauna and macrofauna). The shape function and its expected value should reflect the size and shape of the macrofauna that move sediment nonlocally. Anisotropy can be modeled, for example, by using a shape function that represents directional feeding, such as vertical burrows made by conveyer-belt feeders [1, 4]. The point density should reflect the amount and rate of macrofaunal activity, which in general is depth dependent. The diffusion coefficient should reflect the length and time scales of the meiofaunal activity, which can also be modeled as depth dependent. Assumptions about these parameters will be discussed in the comparison with acoustic data.

3. Seafloor Volume Scattering

The sea floor is modeled as a fluid half-space in which the sediment properties are random functions of space and time. The sediment density and compressibility, ρ_s and κ_s, are defined in terms of their mean and fluctuating components, $\rho_s(\mathbf{r}, t) = \bar{\rho}_s + \delta\rho_s(\mathbf{r}, t)$ and $\kappa_s(\mathbf{r}, t) = \bar{\kappa}_s + \delta\kappa_s(\mathbf{r}, t)$. The water density and compressibility, ρ_w and κ_w, as well as the sediment mean values, $\bar{\rho}_s$ and $\bar{\kappa}_s$, are assumed to be constant in space and time. At the sediment-water interface the density and compressibility are discontinuous, creating an acoustic impedance mismatch. The boundary is in general a rough surface, however, it will be modeled as planar.

A pressure wave, incident upon the sediment, will interact with inhomogeneities in the sediment to create sources of scattered sound, and an integral equation can be obtained by superimposing the induced sources. Thus, for an unbounded region, the resultant scattered field, p', is the sum of the monopole and dipole fields from all the differential sources within the volume of the sediment [9, 10].

$$p'(\mathbf{r}, t) = \int_{V_s} [\bar{k}_s^2(\mathbf{r}')\gamma_\kappa(\mathbf{r}', t)G_0(\mathbf{r}, \mathbf{r}')p(\mathbf{r}', t) - \gamma_\rho(\mathbf{r}', t)\nabla G_0(\mathbf{r}, \mathbf{r}') \cdot \nabla' p(\mathbf{r}', t)] d\mathbf{r}' \tag{9}$$

The average wavenumber in the sediment is defined as $\bar{k}_s^2 = \omega^2 \bar{\rho}_s \bar{\kappa}_s$, where ω is the acoustic frequency. The fluctuating sediment parameters are defined as $\gamma_\kappa = (\kappa_s - \bar{\kappa}_s)/\bar{\kappa}_s$ and $\gamma_\rho = (\rho_s - \bar{\rho}_s)/\rho_s$, and are assumed to vary in time much slower than the acoustic frequency. The Green's function for this system, G_0, is the unperturbed Green's function that satisfies reciprocity and the appropriate boundary conditions along the sediment-water interface. Equation (9) is similar to the well-known integral equation [9] which uses the free-space Green's function. However, in general, G_0 can include gradients in the mean sediment parameters as well as interface effects.

If the field distribution inside the sediment is known, the field outside the sediment can be computed. The total field is the sum of the unperturbed field and the perturbed or scattered field.

$$p(\mathbf{r}, t) = p_0(\mathbf{r}) + p'(\mathbf{r}, t) \tag{10}$$

Equation (9) may be solved by successive approximations using small perturbation theory. Using the known sediment properties and the known Green's function G_0, the total field is expressed as the perturbation series,

$$p(\mathbf{r}, t) = p_0(\mathbf{r}) + p_1(\mathbf{r}, t) + p_2(\mathbf{r}, t) + \cdots , \tag{11}$$

where each higher order term is defined in terms of the preceeding order.

$$p_{n+1}(\mathbf{r},t) = \int_{V_s} [\bar{k}_s^2(\mathbf{r}')\gamma_\kappa(\mathbf{r}',t)G_0(\mathbf{r},\mathbf{r}')p_n(\mathbf{r}',t) - \gamma_\rho(\mathbf{r}',t)\nabla G_0(\mathbf{r},\mathbf{r}')\cdot\nabla' p_n(\mathbf{r}',t)]d\mathbf{r}' \tag{12}$$

If the sediment fluctuations are small, the series converges rapidly and a low-order approximation will sufficiently represent the scattered field.

In the far field and over a small patch of sea floor where it is assumed the incident wave is plane, the half-space Green's function near the interface can be approximated as [11]

$$G_0(\mathbf{r},\mathbf{r}') \simeq \frac{T}{4\pi r} e^{-i\mathbf{k}_w\cdot\mathbf{r}+i\bar{\mathbf{k}}_s\cdot\mathbf{r}'} \quad \text{and} \quad G_0(\mathbf{r}',\mathbf{r}) \simeq \frac{1}{a_\rho}\frac{T}{4\pi r} e^{-i\mathbf{k}_w\cdot\mathbf{r}+i\bar{\mathbf{k}}_s\cdot\mathbf{r}'} \ . \tag{13}$$

T is the pressure transmission coefficient for plane waves incident upon the interface from the water. The position vector $\mathbf{r}$ lies in the water, and $\mathbf{r}'$ lies in the sediment. The origin of the coordinate system is taken on the interface near the center of the region contributing to the integral in (9). The constant a_ρ is necessary to satisfy reciprocity and is defined as the ratio of the average sediment density to water density, $a_\rho = \bar{\rho}_s/\rho_w$. Spherical spreading in the water is included, but neglected in the sediment due to absorption ($r' \ll r$). The wavevector $\mathbf{k}_w$ is in the direction of the incident field, and the wavevector $\bar{\mathbf{k}}_s$ is the corresponding wavevector in the sediment. The transverse components of $\bar{\mathbf{k}}_s$ are the same as those of $\mathbf{k}_w$, and its vertical component is chosen to give the correct sediment wavenumber $\bar{k}_s$. In general the wavenumber in the sediment is complex such that $\bar{k}_s/k_w = (1+i\delta)c_w/\bar{c}_s$, where $\bar{c}_s/c_w$ is the sediment to water sound velocity ratio. The compressional loss factor δ is the ratio of the imaginary to real components of the sediment wavenumber.

Using (12)and (13) the first-order *backscattered* field at position $\mathbf{r}$ in the water is found to be

$$p_1(\mathbf{r},t) = \frac{T^2}{a_\rho(4\pi r)^2}\bar{k}_s^2 e^{-i2\bar{\mathbf{k}}_w\cdot\mathbf{r}} \int_{V_s} [\gamma_\kappa(\mathbf{r}',t) - \gamma_\rho(\mathbf{r}',t)]e^{i2\bar{\mathbf{k}}_s\cdot\mathbf{r}'}d\mathbf{r}' \ . \tag{14}$$

The attenuation in the sediment in the z-direction is determined by $Im[\bar{\mathbf{k}}_s] = k_w Im[P(\theta)]z$. The factor $P(\theta)$ is the ratio of the vertical component of the sediment wavenumber to the wavenumber in the water, $P(\theta) = [(\bar{k}_s/k_w)^2 - \cos^2\theta]^{1/2}$, where θ is the grazing angle in water. The pressure transmission coefficient is $T = 2\zeta/(\zeta+1)$, and the z-direction impedance ratio is $\zeta = (a_\rho \sin\theta)/P(\theta)$.

3.1. Temporal Correlation of the Backscattered Field

As the sediment fluctuates randomly in time, the scattered field will fluctuate. Thus, the backscattered field is also a random process, which can be characterized by the cross-correlation of p_1 at two different times, $R_{pp}(\tau) = \langle p_1(\mathbf{r},t)p_1^*(\mathbf{r},t+\tau)\rangle$. In developing the field correlation we will assume that sediment fluctuations are small, stationary in time, and spatially stationary in the horizontal plane only. The latter two assumptions follow from the sediment model of Section 2. Therefore, assuming the sediment can be approximated as a depth-dependent, but otherwise stationary random processes, the correlation of the first-order backscattered field is found to be

$$R_{pp}(\tau) = \frac{1}{a_\rho^2}\frac{|T^2|^2}{(4\pi r)^4}|\bar{k}_s|^4 \int_{V_s} e^{4Im[\bar{\mathbf{k}}_s]\cdot\mathbf{r}_c}d\mathbf{r}_c \int_{V_s} R(\mathbf{r}_d,z_c,\tau)e^{-i2Re[\bar{\mathbf{k}}_s]\cdot\mathbf{r}_d}d\mathbf{r}_d \ , \tag{15}$$

where the sediment correlation functions appearing in

$$R(\mathbf{r}_d,z_c,\tau) = R_{\kappa\kappa}(\mathbf{r}_d,z_c,\tau) - 2R_{\kappa\rho}(\mathbf{r}_d,z_c,\tau) + R_{\rho\rho}(\mathbf{r}_d,z_c,\tau) \ . \tag{16}$$

are the auto- and cross-correlations of the zero-mean functions γ_κ and γ_ρ. The difference and center coordinates are defined as $\mathbf{r}_d = \mathbf{r}_1 - \mathbf{r}_2$, and $\mathbf{r}_c = (\mathbf{r}_1+\mathbf{r}_2)/2$, respectively. Following other authors [12], we assume the sediment compressibility fluctuations are proportional to the density fluctuations, $\gamma_\kappa = \mu\gamma_\rho$. The sign of the proportionality constant μ is positive if ρ_s and κ_s are positively correlated and negative if negatively correlated [12, 13].

Applying the above assumptions, the Wiener-Khintchin theorem, and the Fourier windowing theorem, the correlation function (15) can be expressed as

$$R_{pp}(\tau) = \frac{A}{a_\rho^2}\frac{|T^2|^2}{32\pi r^4}|\bar{k}_s|^4(\mu-1)^2 \int_{-\infty}^{0} \tilde{S}_{\rho\rho}(\mathbf{k}_d,z_c,\tau)e^{4\alpha z_c}dz_c \ , \tag{17}$$

where A is the area of the scattering region and $\mathbf{k}_d = 2Re[\bar{\mathbf{k}}_s]$ is the Bragg wavenumber having magnitude $k_d = 2k_w[\cos^2\theta + (Re[P(\theta)])^2]^{1/2}$. The imaginary component of the vertical wavenumber is $\alpha = Im[\bar{\mathbf{k}}_s] \cdot \hat{z}$, or, using previous notation, $\alpha = k_w Im[P(\theta)]$. The modified density spectrum, $\tilde{S}_{\rho\rho}$, is the convolution of the true density spectrum and the Fourier transform of the half-space window.

$$\tilde{S}_{\rho\rho}(\mathbf{k}_d, z_c, \tau) = \int_{-\infty}^{\infty} S_{\rho\rho}(\mathbf{k}'_d, z_c, \tau) W(k'_z - k_z, z_c) dk'_z \tag{18}$$

The half-space window function, defined in the difference coordinates, is a depth-dependent rectangular window having the Fourier transform

$$W(k_z, z_c) = \frac{\sin(2k_z z_c)}{\pi k_z}. \tag{19}$$

Therefore, the convolution integration of (18) is only over the z-component of the Bragg wavenumber.

3.2. Backscatter Strength

The first-order backscatter strength is defined in terms of the zero-lag correlation of the backscattered field. If the penetration distance into the sediment is small compared to the distance traveled in water ($r' \ll r$), it is typical to describe volume scattering in terms of an equivalent surface scattering strength. From (17) the surface backscatter strength is found to be

$$\sigma_s = \frac{\pi}{2} \frac{|T^2|^2}{a_\rho^2} |\bar{k}_s|^4 (\mu - 1)^2 \int_{-\infty}^{0} \tilde{S}_{\rho\rho}(\mathbf{k}_d, z_c) e^{4\alpha z_c} dz_c \ . \tag{20}$$

This expression for scattering strength is similar to those derived by [11, 12, 13, 14], except half space effects are included. The half-space windowing effect, expressed as the convolution integral in (18), can be interpreted as a smoothing of the density spectrum. Insight into this effect is gained by combining (20) (18) and (19) and assuming the density spectrum is independent of depth. By performing the integration over z_c, a new window is defined.

$$\tilde{W}(k_z) = \frac{1}{2\pi(4\alpha^2 + k_z^2)} \tag{21}$$

If the spectral representation of the half-space window is a narrow function compared to the spectrum of sediment inhomogeneities, the convolution will have little smoothing effect, and the half-space effects are negligible. However, for certain combinations of grazing angle and attenuation, the window is broad and the convolution may significantly alter the density spectrum at the wavenumbers of interest.

4. Model-Data Comparison

Acoustic backscatter data and sediment physical properties were measured in a shallow bay of Orcas Island, Washington State, USA in August 1995. A calibrated 40 kHz monostatic transducer with a fan-shaped beam pattern was used to scan a site approximately 50 meters in radius. The instrument remained at a fixed location for approximately 60 days. Each day, 10 complete circular scans of the site were recorded. The complete acoustic data set provides a series of backscatter images that reveal changes in the sediment occurring over the time and distance scales of the experiment.

The sediment in the area is a silty-clay with moderate biologically activity. No bubbles were observed in the sediment, and an extensive set of sediment physical properties were measured at the site by investigators of the US Naval Research Laboratory. This work included core and in-situ measurement of geoacoustic parameters, X-radiography of sediment inhomogeneity, and stereophotographic measurement of sea floor roughness.

4.1. Backscatter Strength

Backscatter strength per unit area of sea floor was measured as a function of grazing angle for the Orcas site. The scattering mechanism cannot be inferred from the acoustic data only, owing to the similarity of the magnitude and angular dependence of the measured values compared to other sites having a range of different sediment types [7, 12, 15, 16, 17, 18]. By using sediment measurements as inputs to models for acoustic scattering, the model results are compared with observed backscatter data, and the dominant scattering mechanism inferred.

Two scattering models are considered: scattering from volume inhomogeneities and scattering from a rough sediment-water interface. Both models assume a fluid sediment. Surface roughness scattering is treated using a

Density Ratio	a_ρ	1.406	Diffusion Coefficient	D_0	2.4 $(cm^2/year)$
Sound Velocity Ratio	$\bar{c}_s/c_w$	0.977	Macrofauna Rework Depth	L_λ	3.8 (cm)
Proportionality Constant	μ	-0.934	Meiofauna Rework Depth	L	3.8 (cm)
Compressional Loss	δ	0.0019	Mean Radius	η_a	0.4 (cm)
Spectral Strength	w_3	6.443e-05 (cm^{-1})	Radius Standard Deviation	σ_a	0.14 (cm)
Correlation Length	l_c	3.198 (cm)			

Table 1: Sediment parameters estimated from cores and model-data comparison for the Orcas site.

first-order perturbation approximation [12] with roughness characterized by the two-dimensional, isotropic, power-law spectrum estimated from sites with similar sediments [7, 12]. The Orcas roughness data have not yet been analyzed. As Figure 2 shows, the predicted interface scattering was sufficiently below the measured values that interface scattering effects can be safely neglected, even without full knowledge of the actual roughness parameters.

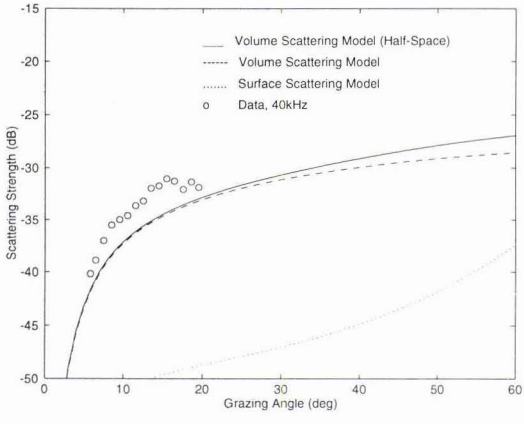

Figure 2: Comparison of measured backscatter with model predictions for the Orcas site.

Volume scattering is treated in a manner similar to Section 3.2 except that the sediment fluctuations are not treated as depth-dependent, owing to lack of resolution in the core data. For the special case of a depth-independent density spectrum and neglecting half-space effects, (20) can be rewritten as

$$\sigma_s = \frac{|T^2|^2}{4\alpha a_\rho^2}\sigma_v \tag{22}$$

where σ_v is the sediment volume backscatter strength.

$$\sigma_v = \frac{\pi}{2}|\bar{k}_s|^4(\mu-1)^2 S_{\rho\rho}(\mathbf{k}_d) \tag{23}$$

Figure 2 shows the predicted backscatter strengths found using the first-order volume model of (20) and (21) which include half-space effects effects, and using (22) and (23) without half-space effects. In this case, a first-order approximation models the data reasonably well, and half-space effects can be negligible. The difference between model predictions and data is most likely due to errors in the estimated inhomogeneity spectra.

Following [19], the spectra of core density fluctuations were estimated using a first-order auto-regressive (AR) model applied to the Orcas core data. This model assumes that the auto-correlation of the normalized fluctuations (taking density as an example) can be expressed as

$$R_{\rho\rho}(\mathbf{r}_d) = \sigma_\rho^2 e^{-|\mathbf{r}_d|\ln\hat{a}}\ , \tag{24}$$

where $\hat{a}$ is the first order AR coefficient estimated from the core data using the Levinson-Durbin algorithm [20]. Since γ_ρ is a zero-mean process, the zero-lag autocorrelation is its variance σ_ρ^2. The three-dimensional density spectrum is found from (24) to be

$$S_{\rho\rho}(k) = \frac{w_3}{(1/l_c^2 + k^2)^2}\ , \tag{25}$$

where l_c is the correlation length defined as $l_c = -\delta z/\ln\hat{a}$, δz is the core sampling interval, and $w_3 = {\sigma_\rho}^2/(\pi^2 l_c)$. Similar expressions are used for the compressibility spectrum and cross-spectrum. The spectral parameters for the Orcas cores are listed in Table 1 along with other geoacoustic parameters supplied by [21]. While these data give reasonable agreement between the acoustic model and data, there are concerns as to the sufficiency of the core inhomogeneity data. The core sampling interval of 2 cm provides marginal resolution compared to the acoustic wavelength. Also, the core data are one-dimensional, which necessitated an assumption of isotropy in the spectral estimates. Both of these concerns could be addressed through use of X-ray data obtained during the Orcas experiment [22, 23].

4.2. Backscatter Correlation

The coherent correlation of the backscattered field is used to observe the changing sediment. First, the complex envelope of the received signal, $s(t)$, is digitized and range-gated to correspond with small patches of sea floor.

Next, the signal from each range bin is cross-correlated with the signal from the same range bin, but from a later scan.

$$R_{ss}(\tau) = \sum_{n=M}^{M+N-1} s_0(t_n) s_\tau^*(t_n) e^{i\frac{\delta c}{c}\omega t_n} \tag{26}$$

The subscript on s denotes the scan time; s_0 is the signal from the scan chosen as a reference, and s_τ is the signal from a scan at time τ later. Sound velocity fluctuations in the water, δc, are compensated by a correction to the phase of the received signal [24]. This phase correction was estimated from sound speed measurements obtained using a conductivity and temperature instrument mounted on the acoustic platform. No significant oceanographic processes or sediment transport events were observed during the experiment. For the Orcas site, sound speed fluctuations were not a significant factor in the observed changes in the backscattered field. Given the nature of the sediment and the expected low level of roughness scattering, it is expected that acoustic penetration into the sediment and the effects of biological mixing are the dominant mechanism for decorrelation.

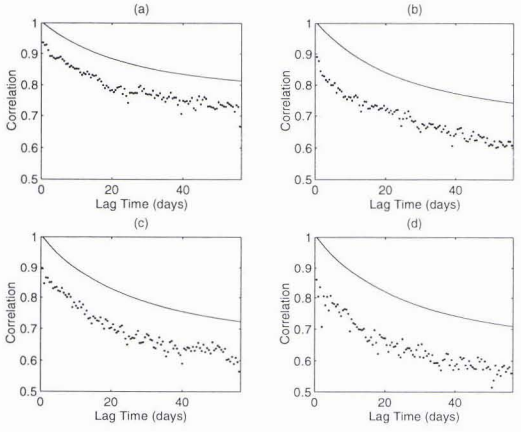

Figure 3: Comparison of measured backscatter correlation and model predictions, (a) $\theta = 14.7°$, (b) $\theta = 9.4°$, (c) $\theta = 7.6°$, (d) $\theta = 6°$

Predictions of the backscatter correlation using the models of Sections 2 and 3.1 are compared with the correlation estimated from the Orcas backscatter data. In this comparison, several simplifying assumptions about the sediment model are made. First, a simple spherical shape function is used, such that

$$H_n(k) = \frac{1}{2\pi^2 k^3}(\sin ak - ak\cos ak) \ . \tag{27}$$

The radius a is a Gaussian random variable with normal distribution $N(\eta_a; \sigma_a)$. The depth-dependent point density and diffusion coefficient are modeled as

$$\lambda(z) = \lambda_0 e^{-z^2/L_\lambda^2} \quad \text{and} \quad D(z) = D_0 e^{-z^2/L^2} \tag{28}$$

where the activity decreases with depth at a rate defined by the macrofauna and meiofauna rework depths L_λ and L.

Using (27), (28), and (17- 19), the normalized correlation coefficient is calculated. In general, the convolution and the expected value integral must be performed numerically. Figure 3 shows a comparison of the observed and predicted correlations as functions of lag time. The model was fitted to the data (plotted as points) by trial and error while constraining the parameters of the sediment model to realistic values. The offset is due to uncorrelated noise in the data. Table 1 outlines the parameters estimated from the model-data comparison. These values are presented mainly as an illustration of the model. Further work is required before bioturbation parameters can be estimated with confidence from acoustic backscatter data.

5. Summary

A model for the change in correlation of sea floor backscattering as a function of the time has been presented. We combine a diffusion model having random excitation to describe the time evolution of sediment inhomogeneities and a first-order perturbation treatment of sediment volume backscatter. The first-order volume backscatter model is validated by comparison with acoustic data using sediment inhomogeneity spectra measured from core data. This model includes half-space effects which were found to be negligible in the present case, but which could affect correlation estimates. Higher resolution two- or three-dimensional core analysis (X-ray, CT) is recommended for future work to reduce errors in application of the scattering model. The backscatter correlation model predicts sediment bio-diffusion parameters that are realistic, but further work is needed in which acoustically derived parameters are compared with ground truth.

Acknowledgments

This work was sponsored by the US Office of Naval Research through the Coastal Benthic Boundary Layer Program and through Codes 321OA and 322BC. The authors are indebted to Dr. Kevin Briggs and Dr. Michael Richardson of the US Naval Research Laboratory for supplying some of their unpublished data and to Dr. Peter Jumars who conceived and led the Orcas experiment.

References

[1] P. A. Jumars. *Concepts in Biological Oceanography*, New York, Oxford University Press, 1993.

[2] R. A. Wheatcroft, P. A. Jumars, C. A. Smith, A. R. Nowell, "A Mechanistic view of particulate biodiffusion coefficient: Step lengths, rest periods and transport directions," *J. Mar. Res.*, 48, 177-207, 1990.

[3] R. A. Wheatcroft, C. A. Smith, P. A. Jumars, "Dynamics of surficial trace assemblages in the deep sea" *Deep-Sea Res..*, vol. 36, no. 1, 71-91, 1989.

[4] B. P. Boudreau, "Mathematics of tracer mixing in sediments: III. The theory of nonlocal mixing within the sediment," *Am. J. Sci.*, vol. 287, p. 693-719, September 1987.

[5] C. de Moustier, D. Alexandrou, "Angular dependence of 12 kHz seafloor acoustic backscatter," *J. Acoust. Soc. Am.*, vol. 90, pp. 522-531, July 1991.

[6] H, Matsumoto, R. P. Dziak, C. G. Fox, "Estimation of microtopographic roughness through modeling of acoustic backscatter data recorded by multibeam sonar systems," *J. Acoust. Soc. Am.*, vol 94, pp. 2776-2787, November 1993.

[7] D. R. Jackson, K. B. Briggs, "High-frequency bottom backscattering: Roughness versus sediment volume scattering," *J. Acoust. Soc. Am.*, vol. 92, pp. 962-977, August 1992.

[8] A. Papoulis, *Probability, Random Variables, and Stochastic Processes*, New York, McGraw-Hill Inc., 1991.

[9] P. M. Morse, K. U. Ingard, *Theoretical Acoustics*, Princeton University Press, New Jersy, pp. 410, 1968.

[10] A. N. Ivakin, "A unified approach to volume and roughness scattering," unpublished.

[11] A. N. Ivakin, Yu. P. Lysanov. "Underwater sound scattering by volume inhomogeneities of a bottom medium bounded by a rough surface," *Sov. Phys. Acoust.*, vol. 27, May-June 1981.

[12] D. R. Jackson, K. B. Briggs, K. Williams, M. Richardson, "Tests of models of high-frequency seafloor backscatter," *IEEE Journal of Oceanic Engineering*, vol. 21, no. 4, October 1996.

[13] T. Yamamoto. "Acoustic scattering in the ocean from velocity and density fluctuations in the sediment," *J. Acoust. Soc. Am.*, vol. 99, pp. 866-879, February 1996.

[14] P. C. Hines, "Theoretical model of in-plane scatter from a smooth sediment seabed," *J. Acoust. Soc. Am.*, vol. 88, pp. 325-334, July 1990.

[15] H. Boehme, N. P.. Chotiros, "Acoustic backscattering at low grazing angles from the ocean bottom," *J. Acoust. Soc. Am.*, vol. 84, pp. 1018-1029, Sept. 1988.

[16] A.V. Bunchuk and Y. Y. Zhitkovski, "Sound scattering by the ocean bottom in shallow-water regions (review)," *Sov. Phys. Acoust*, vol. 26, pp. 363-370, 1980.

[17] P. D. Mourad, D. R. Jackson, "High frequency sonar equation models for bottom backscatter and forward loss," in *Proceedings of OCEAN '89*, IEEE, New York, pp. 1168-1175, September 1989.

[18] M. Gensane, "A statistical study of acoustic signals backscattered from the sea bottom," *IEEE J. Oceanic Engr.*, vol. 14, pp.84-93, 1989.

[19] K. B. Briggs, "High-frequency acoustic scattering from sediment interface and volume inhomogeneities," NRL/FR/ 7431–94-9617, December 1994

[20] J. Proakis, D. Manolakis, *Digital Signal Processing*, New York, Macmillan Publishing Company, pp. 116, 262, 1992.

[21] M. D. Richardson, private communication.

[22] K. B. Briggs, private communication.

[23] T. H. Orsi, private communication.

[24] J.G. Dworski and D. R. Jackson, "Spatial and temporal variation of acoustic backscatter in the STRESS experiment," *J. Continental Shelf Res.*, vol. 14, pp. 1221-1237, August 1994.